Applied Surface Science 464 (2019) 1–9

Contents lists available at ScienceDirect

Applied Surface Science

journal homepage: www.elsevier.com/locate/apsusc

Full Length Article

Mixed RuO_2/TiO_2 uniform microspheres synthesized by low-temperature ultrasonic spray pyrolysis and their advanced electrochemical performances☆

Milica Košević[a], Srecko Stopic[b], Vesna Cvetković[a], Michael Schroeder[c], Jasmina Stevanović[a,d], Vladimir Panić[a,d,e,*], Bernd Friedrich[b]

[a] Institute of Chemistry, Technology and Metallurgy, University of Belgrade, Belgrade, Serbia
[b] IME Process Metallurgy and Metal Recycling, RWTH Aachen University, Germany
[c] Institute of Physical Chemistry of the RWTH Aachen University, Germany
[d] Centre of Excellence in Environmental Chemistry and Engineering – ICTM, University of Belgrade, Belgrade, Serbia
[e] State University of Novi Pazar, Chemical-Technological Department, Novi Pazar, Serbia

ARTICLE INFO

Keywords:
Binary oxides
Electrocatalysis
Composites
Electrochemical impedance
Morphological stability

ABSTRACT

Uniformly-shaped, spherical RuO_2/TiO_2 particles were synthesized exclusively by one-step ultrasonic spray pyrolysis (USP) of a mixture of *n*-butylorthotitanate and ruthenium chloride acidic aqueous solutions. The USP temperature was 200 °C – quite below the typical conversion temperatures of the precursors to the oxides. Basic electrochemical properties of RuO_2/TiO_2 USP powders (as-prepared or additionally dried and/or thermally treated) in the form of a thin layer applied onto glassy carbon electrode are investigated and compared to the properties of powder synthesized at quite higher temperature of 800 °C. The coatings of activated titanium anode (ATA) were prepared from RuO_2/TiO_2 USP powders in order to check the anode electrolysis stability and to correlate the anode properties to those of native USP powders. Low-temperature material showed much better performances than high-temperature one. ATA obtained from low-temperature USP powder showed considerably higher stability. The obtained results are found to be in close correlation to the powder and coating structure, composition and morphology affected by subsequent thermal treatment of the material synthesized at low USP temperature.

1. Introduction

The RuO_2/TiO_2 binary-oxide, or electrochemically more stable RuO_2–IrO_2/TiO_2 ternary-oxide, have attracted attention primarily in chlor-alkali electrolysis due to its excellent electrocatalytic properties in gas-evolving anodic reactions [1]. Activated Ti anodes (ATA) with the coatings of these multicomponent oxides are widely used for industrial chlorine production [2–4], oxygen evolution, direct or indirect electrochemical degradation of organic contaminants in waste water treatment, electrowinning of metals, etc [4–7]. Recently, interest has been expanded to potential application of noble metal oxides in supercapacitators [8–11].

A number of studies has been published on the properties and electrode kinetics of RuO_2/TiO_2 as a catalyst [6–12], it was found that the preparation conditions can influence strongly the coating surface morphology or microstructure of binary oxide and consequently the electrochemical behavior [5,6]. Many of the results suggest that sol-gel method [6–15] for the preparation of ordered RuO_2/TiO_2 coatings is to be beneficial for their properties. Significant improvement of the electrocatalytic activity can be achieved by variety of novel synthetic routes for ultrafine particles of binary metal oxide [16–19].

Bearing in mind these considerations about oxide structure/synthesis relationship, it follows that innovative approaches toward synthesis of binary oxide could be still of high interest. They especially should aim to improve and facilitate the oxide synthesis procedures for highly controllable structures, and consequently design and electrochemical performances of synthesized mixed oxides. In previous works, we presented the synthesis of sub-μm, highly-ordered spherical binary oxide particles in the TiO_2 core–RuO_2 shell, or hierarchical, form, which was achieved by ultrasonic spray pyrolysis (USP) method [17,20,21].

☆ To the memory of Professor Nedeljko Krstajić who passed away in August, 2017. This work is dedicated to the recognition of his outstanding contribution to the knowledge of activated titanium anodes.

* Corresponding author at: Institute of Chemistry, Technology and Metallurgy, University of Belgrade, Njegoševa 12, 11000 Belgrade, Serbia.
E-mail address: panic@ihtm.bg.ac.rs (V. Panić).

https://doi.org/10.1016/j.apsusc.2018.09.066
Received 27 April 2018; Received in revised form 6 September 2018; Accepted 8 September 2018
Available online 08 September 2018
0169-4332/

Most recently [20], we applied coupled USP–electrostatic deposition setup to synthesize RuO_2/TiO_2 particles in a horizontal reactor followed by their application as a coating of industrial ATAs. The synthesized particles were applied onto expanded titanium within a continuous process. The *ex situ* coating of Ti by USP-synthesized binary oxide powder resulted in ATAs of typical electrochemical properties. However, the stability of USP-obtained ATA in electrolysis was not found improved with respect to ATAs synthesized by other procedures reported in the literature [22,23]. On the other hand, the structure of native USP binary oxide is well preserved and reflected into the structure of the coating [20], thus allowing high coating texture control by *ex situ* USP synthesis of the oxides. This indicates that additional modifications of USP conditions are valid prerogatives for the substantial improvement of the ATA coatings, especially their service life, which is believed to depend on coating structure parameters affected by oxide synthesis [7,24].

The initially posed USP conditions [20] have been projected to ensure the conversion of Ru chloride into oxide at the surface of hydrous TiO_2 particles during the pyrolytic spraying at 800 °C and subsequent electrostatic collection of the powder at 500 °C. Hence, the temperature regimes in both the USP furnace and the collecting chamber fulfilled the demand for defined creation of the oxide phases (typically 400–500 °C). Quite moderate service life [20] registered for the USP-prepared ATA could be due to complete conversion to oxides at 800/500 °C and consequently the absence of coating/support transformations required for good coating accretion. The main intention behind this work is to investigate the possibility to synthesize the oxides at enough low USP temperatures, and thus to adjust the desirable USP oxides/Ti substrate interactions. The average USP synthesis temperature was decreased from 800 °C to the far low extreme of 200 °C. A vertical reactor of three different heating zones was employed [21], whereas the electrostatic collection was performed at 120 °C. In addition to the expectation of improved coating/substrate interactions, the decrease in temperature is also beneficial from the standpoint of energy savings during the ATA synthesis. The influence of synthesis temperature on the electrochemical response of both the powders, in a form of thin layer on glassy carbon (GC), and the corresponding ATA coatings, is investigated. Finally, the impact of synthesis temperature to the stability of obtained ATAs is discussed. Detailed electrochemical measurements were done by cyclic voltammetry (CV) and electrochemical impedance spectroscopy (EIS).

2. Experimental

2.1. Synthesis of the RuO_2/TiO_2 powders

The RuO_2/TiO_2 powders were synthesized by ultrasonic spray pyrolysis (USP) at 200 and 800 °C (RuO_2/TiO_2 (2 0 0) and RuO_2/TiO_2(8 0 0), respectively); the methodology is described in previous work [20]. Tetra-*n*-butyl orthotitanate and ruthenium(III) chloride hydrate in hydrochloric acid solution have been used as precursors, which was driven (O_2, 3 L/min) trough vertical tube furnace [21] upon ultrasonic atomization (Gapusol 9001, RBI atomizer, France, operating at 2.5 MHz). The experimental conditions of ultrasonic spray pyrolysis was projected to give 25:75 mol ratio of Ru:Ti. Final calcinations of the powder was performed during its collection in an electrostatic field (30 kV, 0.08 mA) at 120 and 500 °C for RuO_2/TiO_2(2 0 0) and RuO_2/TiO_2(8 0 0), respectively. Finally, the RuO_2/TiO_2 particles have landed in a bottle filled by water, placed at the bottom of electrostatic chamber.

2.2. Preparation of RuO_2/TiO_2 coating of activated titanium anode from synthesized powders

In order to check the properties of synthesized RuO_2/TiO_2 particles as a coating for ATA, Ti substrate was coated as follows [20]. Obtained RuO_2/TiO_2 powders were suspended in 2-propanol (17.5 mg cm^{-3}). The suspension was stabilized by ultrasonic treatment (40 kHz, 70 W) in 15 min and brushed onto Ti rod (3 mm in diameter). Before RuO_2/TiO_2 layer deposition, the titanium surface was etched in hot HCl solution (50 vol.% of conc. HCl in water) for *ca*. 15 min. Coating was deposited from obtained suspension onto prepared Ti substrate in 6 layers. The deposition of each layer consisted of drying of brushed suspension at 120 °C and subsequent annealing at 450 °C for 5 min. Upon deposition of the 6th layer, roughly corresponding to 1 mg cm^{-2} of RuO_2/TiO_2, the ATA was finally annealed at 450 °C for 20 min.

2.3. Electrochemical characterization

The electrochemical response of synthesized RuO_2/TiO_2 powders was gained from their thin layer formation on GC support. The GC-supported layer was obtained from 3 mg cm^{-3} water suspensions pipetted onto a GC disk and dried (room temperature), which gave 0.31 mg RuO_2/TiO_2 per cm^2 of GC. Suspensions were obtained from as-synthesized and thermally-treated RuO_2/TiO_2 powders: air-dried at 120 °C for 24 h and/or annealed at 450 °C for 30 min. The thermal treatments were performed in order to check the influence of thermal regime on the properties of USP-synthesized mixed oxide, as it is going to be applied during the ATA coating preparation. In order to ensure good adhesion of a layer on GC, the room-dried layer was covered with Nafion® (from a solution of 1:100 volume ratio of 10 mass% Nafion® solution in isopropanol:water, left to room-dry upon application over the GC-supported oxide layer).

Cyclic voltammetry (CV) and electrochemical impedance spectroscopy (EIS) measurements were performed in 1.0 M H_2SO_4 in a three-electrode electrochemical cell with GC-supported layer or ATA as working electrodes, saturated calomel electrode as the reference and a Pt plate as counter electrode.

All electrochemical experiments were conducted using potentiostat/galvanostat, model SP-200 (Bio-Logic SAS, France), at room temperature. EIS was recorded with sinusoidal voltage of 10 mV amplitude, in a multisine mode. CV was performed with sweep rate of 50 mV s^{-1}. Electrochemical performances of the ATA were further investigated by the accelerated electrolysis stability test (AEST). AEST of the prepared anode was conducted galvanostatically in 0.5 M NaCl, pH 2, at constant current density of 2.0 A cm^{-2} and 18 °C. Pt plate was used as a cathode. The pH was held constant by the addition of HCl solution. The cell voltage is recorded continuously and the loss of the anode activity is indicated by time required for the cell voltage to start to increase continuously.

3. Results and discussion

3.1. XRD analysis of the powders

Fig. 1 shows XRD spectra of RuO_2/TiO_2(8 0 0) and RuO_2/TiO_2(2 0 0) sample (curves a and b, respectively). The RuO_2/TiO_2(8 0 0) sample is of well-developed crystalline structure, with distinct diffraction peaks corresponding to most intense reflections of rutile, but also of anatase structure (the most intense (1 0 1) reflection at 25.28°) for TiO_2. The XRD pattern of RuO_2/TiO_2 (2 0 0) is of considerably less pronounced crystalline features, and indicates the structure of much amorphous characteristics. In order to perform a detailed analysis of the structure, the characteristic XRD domains were extracted (the insets of Fig. 1) and subjected to provisional Gaussian deconvolution with respect to standard XRD cards for RuO_2 [25] and the rutile and anatase TiO_2 (JCPDS 21-1276 and 21-1272, respectively). The aim was to analyze the possible appearance of distinct TiO_2 and RuO_2 phases as an indication of USP-induced hierarchical ordering of the structure of mixed oxide. An inset of Fig. 1 gives also the intensity-zoomed spectra of the RuO_2/TiO_2(2 0 0) of apparently amorphous structure.

The presence of TiO_2 anatase, as it is clearly observed by the

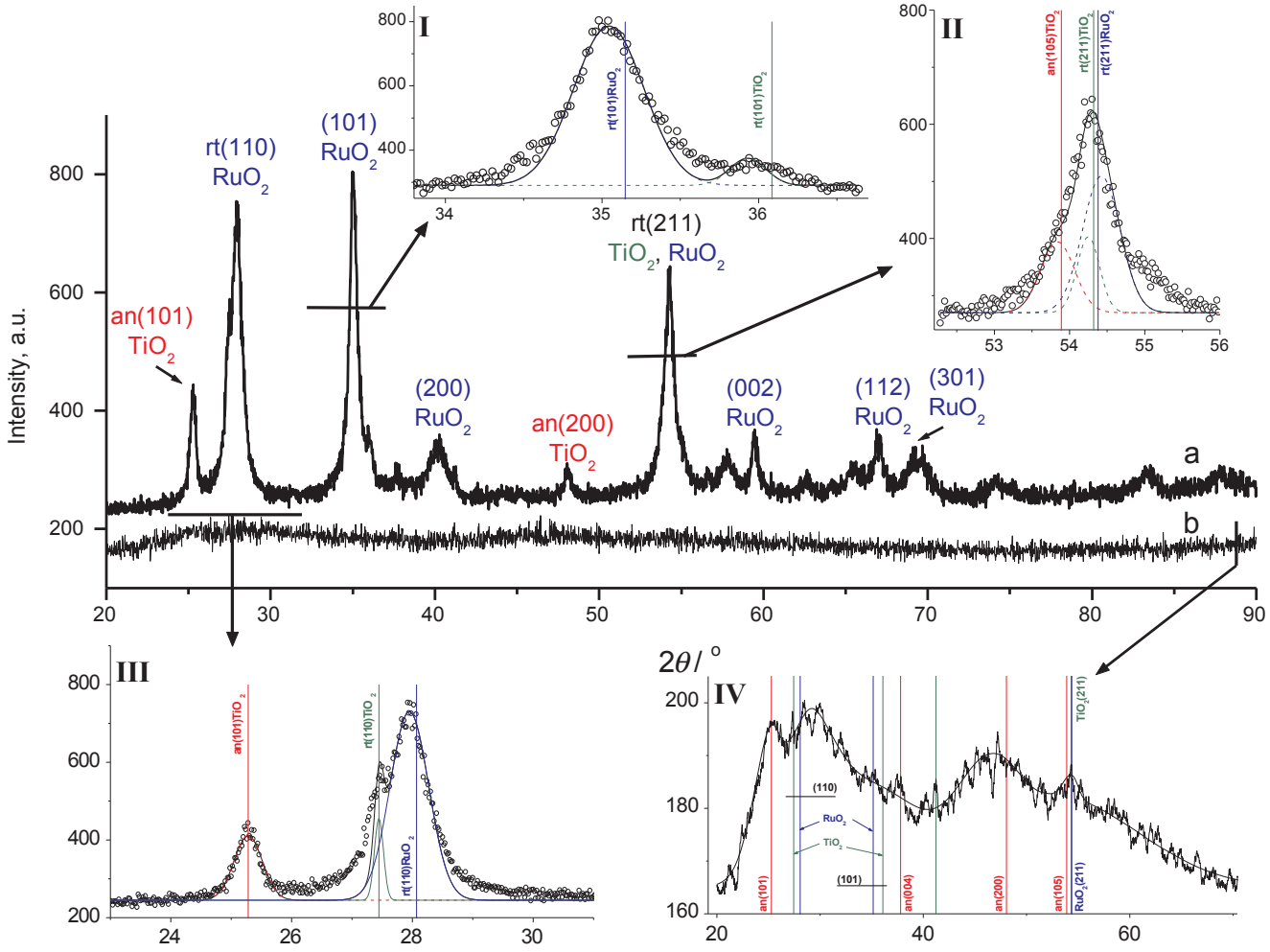

Fig. 1. XRD spectra of: (a) RuO_2/TiO_2(8 0 0) and (b) RuO_2/TiO_2(2 0 0); the insets give the zoomed characteristic parts of the a and b patterns: rutile, I –(1 0 1), II – (2 1 1) and III – (1 1 0) and anatase (1 0 1) reflections of RuO_2/TiO_2(8 0 0); IV – intensity-zoomed pattern of RuO_2/TiO_2(2 0 0).

appearance of its most intense (1 0 1) and (2 0 0) reflections in the XRD pattern of RuO_2/TiO_2(8 0 0) (Fig. 1, curve a), is indicated even in the weakly intense pattern of RuO_2/TiO_2(2 0 0) (Fig. 1, inset IV). Owing to low crystallinity and much wider peaks of RuO_2/TiO_2(2 0 0) in comparison to RuO_2/TiO_2(8 0 0), the anatase (1 0 1) reflection appears overlapped in a higher degree with (1 1 0) rutile TiO_2 and RuO_2 reflections at 27.4 and 28.1°, respectively. A (2 0 0) anatase peak, fairly well separated from other anatase and rutile reflections, appears in RuO_2/TiO_2(2 0 0) pattern in a relative more intense and broader form in comparison to RuO_2/TiO_2(8 0 0) pattern. On the other hand, the RuO_2 reflections of similar low intensity as anatase (2 0 0) is (curve a), cannot be identified in the pattern of low-temperature sample. The presence of amorphous Ru species is thus indicated to possibly define the RuO_2/TiO_2(2 0 0) XRD pattern, which the mixed anatase/rutile TiO_2 strikes through. The presence of crystalline TiO_2 at such a low temperature indicates its early creation by hydrolysis of orthotitanate precursor. These features of the low-temperature sample leave the possibility of the time-distinctive formations of TiO_2 and RuO_2 phases during the USP at higher temperature, and consequently their hierarchical ordering.

Although the increase in USP temperature (800 °C) is expected to be favorable for the complete anatase transition to rutile (typically 500–600 °C) [26], curve a in Fig. 1 clearly shows that anatase phase is preserved while RuO_2 crystalline structure, along with rutile TiO_2, develops during USP. RuO_2 (1 0 1) reflection for the high-temperature sample (curve a) appears the most intense, although it should be by one-fifth less intense [25] with respect to (1 1 0) reflection. Similarly, the intensity of anatase (1 0 1) reflection appears reduced to the half with respect to the intensities of other typical anatase reflections ((2 0 0), curve a, and (1 0 5), inset II). The insets I–III of Fig. 1 show certain selective shifts of the peaks to lower 2θ values with respect to the cards as follows. The rutile (1 1 0) and (1 0 1) reflections, as those closest to, and oriented like the most intense anatase (1 0 1) reflection, are systematically shifted by *ca.* 0.1°. The less pronounced shift was found for rutile (2 1 1) (inset II) that is close to anatase (1 0 5) reflection. On the other hand, the anatase peaks themselves appear not shifted. RuO_2 reflections at higher 2θ values, (0 0 2), (1 1 2) and (3 0 1), are of a bit increased shift of *ca.* 0.15°. Although these features could indicate the distortions of the rutile unit cells due to the formation of the TiO_2–RuO_2 solid solution [27], the observed differences in XRD patterns could be assignable much to located growth of the rutile on top of the anatase phase. The later could cause the weakening of the anatase (1 0 1) reflection since these planes lies below rutile (1 0 1) planes of increased relative intensity. Since XRD spectrum of low-temperature sample shows the presence of crystalline TiO_2 which has grown in the USP precursor state, it can play the role of a germ for the formation of the crystalline RuO_2 during the high temperature treatment. Simultaneously, there is a growth of rutile TiO_2 (inset IV) – initially formed, as well as of that generated from high-temperature anatase–rutile transformation process.

In order to evaluate tentatively the crystallite sizes, the Scherrer Equation was applied to deconvoluted most intense reflections. The size

of anatase and RuO_2 from their distinct (1 0 1) reflections was found similar, 17 and 19 nm, respectively. However, the size of rutile TiO_2 from not well resolved (1 0 1) reflection (Fig. 1, inset III) is indicated upon variable deconvolution as more than a twice larger, 40–60 nm. Although the application of Scherrer method to recorded spectra is not fully reliable, it could be considered as a possible estimation of the crystallite sizes. The mentioned sizes gained from well indicated single reflections are able to reproduce by deconvolution the highly overlapped reflections in the anatase (1 0 5) and rutile (2 1 1) domains (Fig. 1, inset II). Calculated sizes indicate that RuO_2 phase can possibly grow on anatase (1 0 1) and subsequently transfers into polycrystalline structure. Larger rutile TiO_2 crystallites could originate from the growth of those initially present (Fig. 1, inset IV), which is caused by subsequent anatase/rutile transformation at higher temperature.

Above mentioned findings seem important, since the co-existence of the rutile and anatase structure in TiO_2/RuO_2 mixed oxide could be of interest as precursor for ATA coatings, which are exclusively obtained as rutile mixed oxide [28]. This proves that applied synthesis procedure is able to generate TiO_2 in the anatase form, which is preserved subsequently during the joined pyrolysis of TiO_2 and $RuCl_3$ at the temperatures as high as 800 °C and required for stable formation of mixed oxides. These structural issues can affect the activity of the mixed oxide, and consequently the stability of ATA coatings.

3.2. SEM/EDX analysis of RuO_2/TiO_2 as-synthesized powders

As expected for spray pyrolysis synthesis of RuO_2/TiO_2 powders [17,20], huge spherical shapes are generated in both RuO_2/TiO_2(2 0 0) and RuO_2/TiO_2(8 0 0) cases, as shown by SEM analysis presented in Fig. 2. These agglomerates, consisted of the clusters of non-uniform size and shape distribution, appeared slightly smaller for RuO_2/TiO_2(8 0 0) sample. The apparent smaller size of RuO_2/TiO_2(8 0 0) agglomerates with respect to RuO_2/TiO_2(2 0 0) ones seems to be due to more pronounced clustering, and hence with the former appearing like more compact. In spite of more compact appearance, SEM image of RuO_2/TiO_2(8 0 0) sample shows more out-of-spheres exfoliated material. It could be that sticking force between clearly separated clusters of TiO_2/RuO_2(2 0 0) is stronger than between rigid, consistently puzzled, parts of RuO_2/TiO_2(8 0 0) agglomerates.

The results of EDX analysis of RuO_2-TiO_2 powders, performed at the twice larger scan size with respect to that used to record the SEM micrographs from Fig. 2, are given in Table 1. Although experimental setup of USP was projected to give 25:75 mol ratio of Ru:Ti, surface Ru content in powders is found higher than projected. This indicates that TiO_2 could be coated by RuO_2 that masks partially the EDX reflection of TiO_2 beneath, as indicated by the analysis of XRD data. RuO_2/TiO_2(8 0 0) sample showed higher Ru content than RuO_2/TiO_2(2 0 0) sample since not all of $RuCl_3$ in RuO_2/TiO_2(2 0 0) was transferred to RuO_2 during synthesis. The presence of 8.5% of chlorine in final powder confirms that the formation of RuO_2/TiO_2 is not complete. As mentioned in experimental part, the obtained material was collected in a bottle filled by water after synthesis. Thus, it could be that some part of the Ru from non-pyrolyzed $RuCl_3$ was redissolved in water and lost. In addition, amorphous $RuCl_3$ could allow EDX beam to penetrate deeper through sample, and hence more TiO_2 beneath RuO_2 shell could reflect the beam. Anyhow, Ru content found in RuO_2/TiO_2(2 0 0) is still higher than projected one, which indicates that masking effect of the RuO_2 is dominant over incomplete chloride/oxide transition at low temperature.

Table 1
Mean values of EDX results (deviations do not exceed 10%) of as-synthesized RuO_2/TiO_2 particles (at. %).

Sample	Element				Ru:Ti ratio
	Ti	Ru	O	Cl	
RuO_2/TiO_2(8 0 0)	17	23	60	–	58:42
RuO_2/TiO_2(2 0 0)	15	9.4	67	8.5	39:61

3.3. FTIR analysis

The intrinsic structure of the USP-synthesized powders, as indicated by XRD and EDX analysis, is checked for the IR response of oxygen-involving bonds by FTIR. FTIR spectra of synthesized RuO_2/TiO_2 powders and commercial RuO_2 are shown in Fig. 3.

All samples show pronounced absorption peaks of different structure and complexity in low wavenumber range (below 1000 cm^{-1}) associated to oxide-typical metal–oxygen (M—O) bond vibration [29-31]. This peak spends the widest wavenumber range in the spectrum of RuO_2/TiO_2(2 0 0) sample, which was registered also in some literature cases for anatase TiO_2 [32,33]. The peaks corresponding to the surface adsorbed water and hydroxyl groups [34], *i.e.*, O—H deformation vibration [35], appear between 1300 and 1700 cm^{-1} (Fig. 3a). It can be observed that these peaks are the least intense, relatively to M—O absorptions, for the sample synthesized at 800 °C due to highest pyrolysis temperature. Similarly, they are relatively the most intense for TiO_2/RuO_2(2 0 0). The higher the temperature, the more pronounced removal of absorbed (residual) water from the RuO_2/TiO_2 structure is.

The structure of the spectra in M—O absorption region can be additionally analyzed by Gaussian deconvolution tool applied to the RuO_2/TiO_2(8 0 0) sample and by comparison to the spectra of commercial RuO_2 and RuO_2/TiO_2(2 0 0) in a corresponding wavenumber range, Fig. 3b. FTIR response of RuO_2/TiO_2(8 0 0) in 400–900 cm^{-1} region appears of complex structure, comprising of well-defined peak at 635 cm^{-1} and a shoulder around 462 cm^{-1}, as well as a weak shoulder around 547 cm^{-1}. Well-defined peak for RuO_2 appears on fairly similar

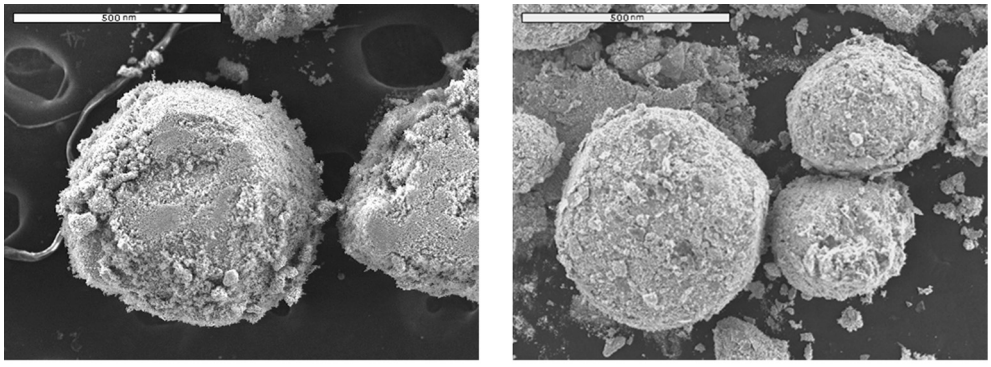

Fig. 2. SEM images of RuO_2/TiO_2 particles synthesized at 200 (a) and 800 °C (b).

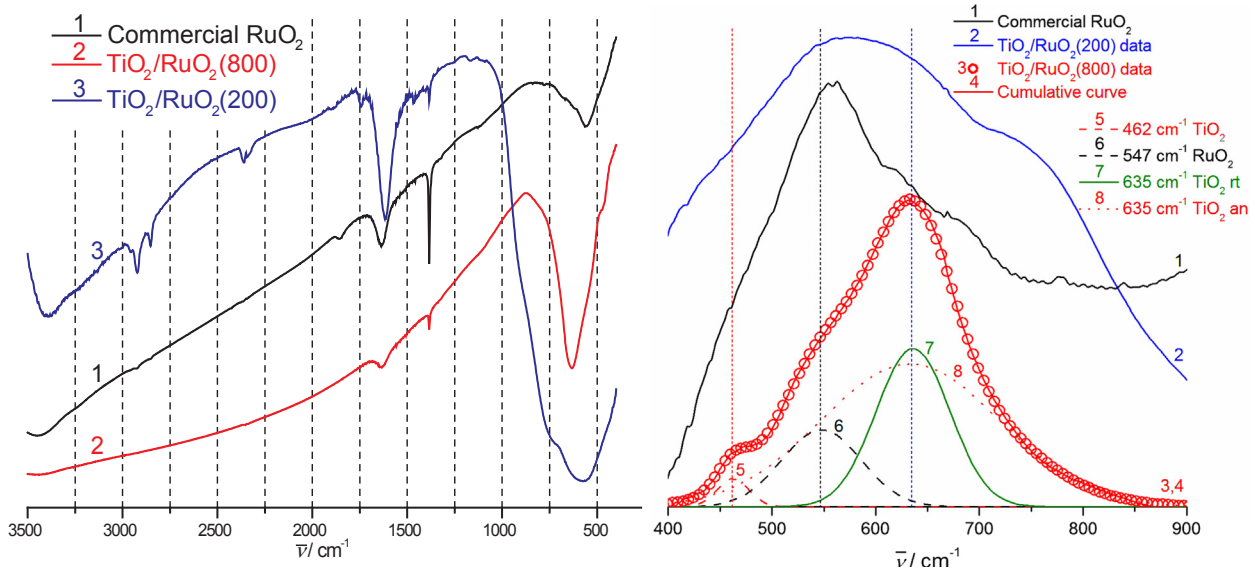

Fig. 3. (a) FTIR spectra of RuO_2/TiO_2(2 0 0), RuO_2/TiO_2(8 0 0) and commercial RuO_2 (transmittance); (b) Comparison of the metal–oxygen absorption regions, with the Gaussian deconvolution of the regional FTIR spectrum of RuO_2/TiO_2(8 0 0) (absorbance).

position of this weak shoulder, while well-defined position for RuO_2/TiO_2(8 0 0) at 635 cm^{-1} is seen only as a very weak shoulder for RuO_2. In the region of mentioned spectra features, the spectrum of RuO_2/TiO_2(2 0 0) sample presents the broad peak of rather highly overlapped absorptions, with additional shoulder around 750 cm^{-1}. The spectral curve of RuO_2/TiO_2(8 0 0) in M—O region can be well reproduced by four Gaussian peaks at the positions associated with the features of the spectra of RuO_2/TiO_2(2 0 0) and RuO_2 (Fig. 3b). Sharp peak 8 and the broad one, 7, form the well-pronounced peak for RuO_2/TiO_2(8 0 0), as well as weak shoulder and a part of the broad absorption for RuO_2 and RuO_2/TiO_2(2 0 0), respectively. Peak 6, which is well pronounced for RuO_2, is associable to Ru—O bond, and apparently forms the joint absorption of RuO_2/TiO_2(2 0 0) with peaks 7 and 8, leaving the possibility for these peaks to be associated to Ti—O and mixed Ti(Ru)—O bonds. The assignments to peak 5 are hard straightforwardly indicated, although it can be considered to correspond much to the shoulder of RuO_2/TiO_2(2 0 0) than to tiny appearing one in RuO_2 spectrum. Bearing in mind that anatase structure can absorb in much wider region than rutile [32,33], rather wide peaks 5 and 8 could be considered as more indicative of Ti—O anatase bond. Hence, they can appear wider in the spectrum of more hydrated RuO_2/TiO_2(2 0 0) with respect to the spectrum of RuO_2/TiO_2(8 0 0). It follows that registered FTIR spectra reflect well the XRD and EDX findings, and corresponding discussion, of mixed anatase–rutile structure.

XRD- and FTIR-related findings and considerations were additionally checked by Raman measurements, which are presented and discussed in Supplementary material.

3.4. TGA analysis

In order to check the hydrous form and chloride–oxide conversion (which appeared not to be complete for RuO_2/TiO_2(2 0 0)) degree, thermogravimetric analysis (TGA) was performed. Fig. 4 shows the TGA curves of RuO_2/TiO_2(2 0 0) and RuO_2/TiO_2(8 0 0) sample. TiO_2/RuO_2(8 0 0) sample exhibited the loss of only 3–4 mass% up to 600 °C, which indicates its rather dry state and complete conversion to crystalline oxide structure. However, RuO_2/TiO_2(2 0 0) loses almost 25% of the initial mass within three main temperature regions. There is a rather fast loss of around 7 mass % up to 100 °C due to sample drying, which is followed by additional loss of around 7 mass % up to 300 °C. This indicates that the mixed oxide is synthesized as hydrous, with strongly bonded crystalline water.

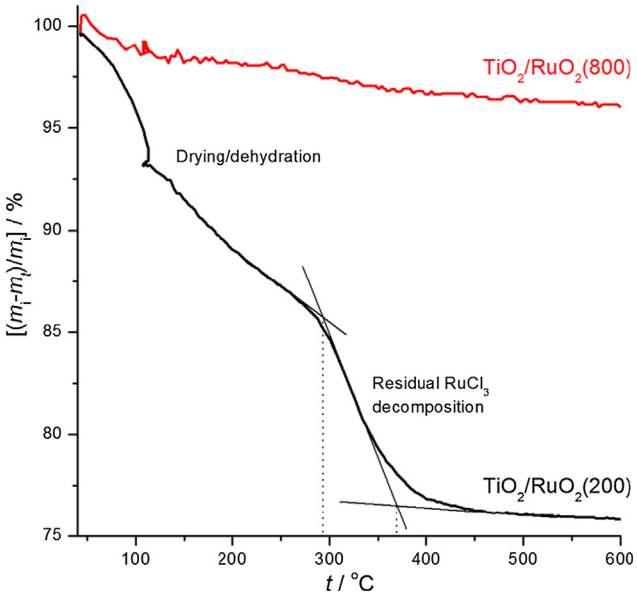

Fig. 4. TGA curves as the residual mass (m_t) in % with respect to initial mass, m_i, of RuO_2/TiO_2(2 0 0) and RuO_2/TiO_2(8 0 0) samples.

The registered loss appears low for the removal of one water molecule from both oxides present. If it would be assumed that TiO_2 is formed in non-hydrous state, then complete loss of water between 100 and 300 °C could originate from the hydrous form of RuO_xH_y, which is known upon strong affinity towards strongly-bonded water at low synthesis temperatures. With this assumption, registered mass loss corresponds to the loss of 0.8–0.9 mol of water from hydrous RuO_2, which is quite close to its monohydrated state. At the temperatures above 300 °C, the final 10% mass loss was registered up to 400 °C. This temperature range is known for the conversion of noble metal chlorides to oxides, especially for $RuCl_3$ [28]. This shows that not complete amount of chlorides is converted to oxides at lower USP synthesis temperature. This was also found by EDX analysis. Residual $RuCl_3$ could act as a kind of a "glue" for the converted material, which can cause the obtained spheres (Fig. 2) as main constituents of the synthesized RuO_2/TiO_2(2 0 0) powder to appear bigger and more compact.

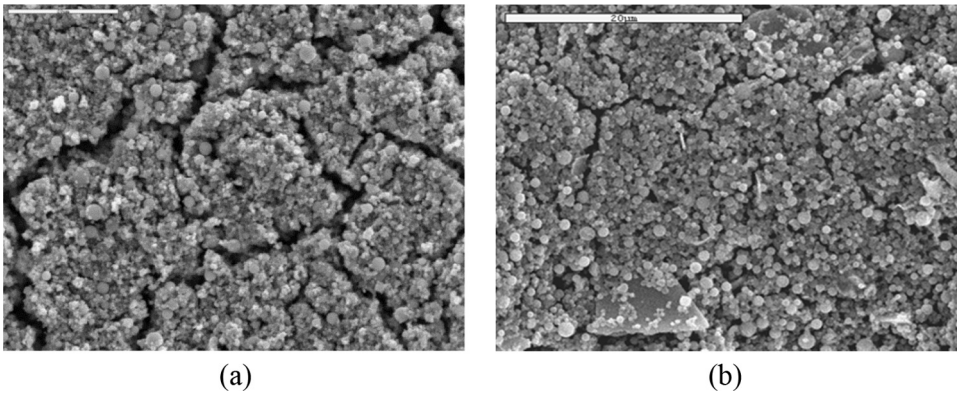

Fig. 5. SEM images of ATA coatings prepared from USP RuO_2/TiO_2 powders synthesized at 200 (a) and 800 °C (b); the bar is 20 μm in length.

3.5. SEM surface appearance of RuO_2/TiO_2(2 0 0)/Ti and RuO_2/TiO_2(8 0 0)/Ti electrodes

Surface morphology of the ATAs coatings, prepared from the suspensions of RuO_2/TiO_2(2 0 0) and RuO_2/TiO_2(8 0 0) USP powders, was investigated by SEM analysis. Typical surface appearances are shown in Fig. 5.

Both coatings wear cracked structure with defined spherical-particle structure of the islands. The USP synthesis procedure apparently generates stable and compact, poorly interactive, spheres affected neither by sonication (during the preparation of a suspension) nor by annealing of the coating. The surface of the RuO_2/TiO_2(2 0 0)/Ti electrode appears of much wider cracks and larger islands (note that magnification in Fig. 5b is *ca.* three times larger). On the other hand, the presence of the resolved spheres seems more frequent in case of RuO_2/TiO_2(8 0 0)/Ti electrode surface. In relation to the appearance of the native RuO_2/TiO_2(8 0 0) powder (Fig. 2b), it can be observed that those middle size particles contribute to more rugged area of the crack walls, edged by mentioned middle size particles. On the other hand, a bit larger particles were sporadically observed in RuO_2/TiO_2(2 0 0) sample, in contrast to RuO_2/TiO_2(8 0 0) sample.

3.6. Electrochemical characterization

The cyclic voltammograms of the ATAs with the coatings made of RuO_2/TiO_2 USP powders synthesized at different temperatures, as well as of their thin layers on glassy carbon (GC) as-synthesized, dried (RuO_2/TiO_2(8 0 0)) and annealed (RuO_2/TiO_2(8 0 0) and RuO_2/TiO_2(2 0 0)) are presented in Fig. 6. Thin layers of as-synthesized and dried variants of RuO_2/TiO_2(2 0 0) were instable in the electrolyte and hence not suitable for electrochemical testing. All voltammograms are of typical shape for RuO_2-containing electrode materials and RuO_2/TiO_2 ATA coatings [36,37]. Higher current densities are registered for RuO_2/TiO_2(2 0 0) in comparison to RuO_2/TiO_2(8 0 0) sample in the annealed state (Fig. 6a), although the surface RuO_2 content was found lower than in RuO_2/TiO_2(8 0 0) sample (Table 1). It appears that the structure of the USP-synthesized RuO_2/TiO_2(2 0 0) is beneficial for the improvement of the TiO_2 role of electrochemical surface area developer [38]. RuO_2 as the active component is better distributed throughout the TiO_2 matrix for the lower RuO_2 content as found in RuO_2/TiO_2(2 0 0) sample, and consequently more efficiently exposed to the electrolyte. Better exposition of the coating should be also expected according to Fig. 5, since the cracks were found much wider for RuO_2/TiO_2(2 0 0).

Another consequence of the different coating compositions exposed to the electrolyte in RuO_2/TiO_2(8 0 0) and RuO_2/TiO_2(2 0 0) samples, as indicated by EDX data, is the voltammetric features at the potentials negative to 0.1 V. While cathodic current continuously increases from 0.4 V toward the cathodic cycling limit in case of RuO_2/TiO_2(2 0 0) (*i.e.*, for lower RuO_2 surface content), there is much better defined increase

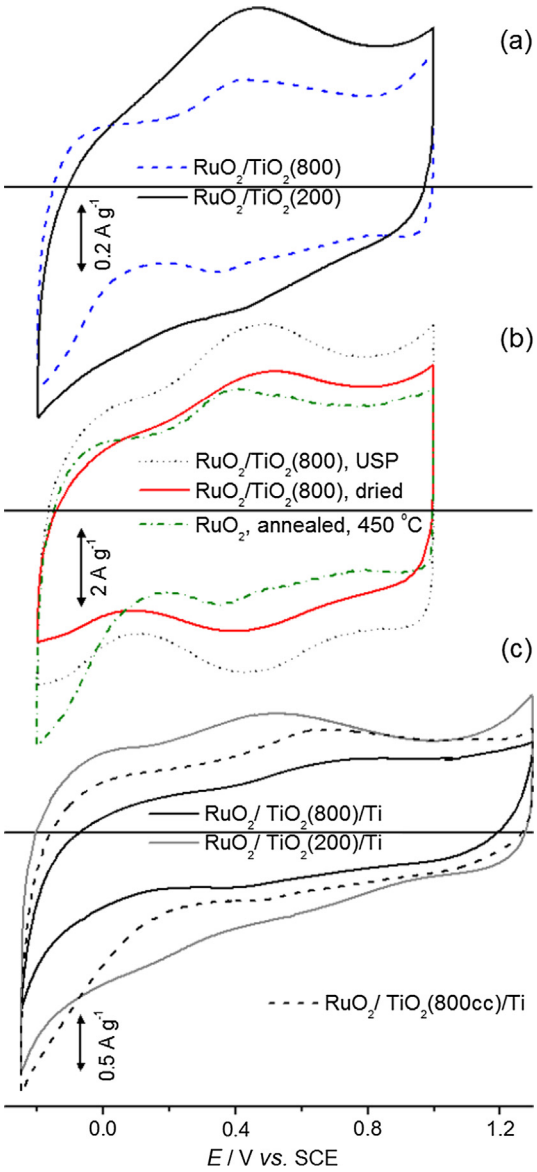

Fig. 6. Cyclic voltammograms of: (a) the layers on GC of annealed RuO_2/TiO_2 powders, (b) as-synthesized and dried RuO_2/TiO_2(8 0 0) and commercial RuO_2 powder annealed, and (c) the RuO_2/TiO_2(2 0 0) and RuO_2/TiO_2(8 0 0) ATA coatings; RuO_2/TiO_2(800 cc)/Ti denotes the coating with composition corrected to that of RuO_2/TiO_2(2 0 0); 1.0 M H_2SO_4, 50 mV/s.

for RuO_2/TiO_2(8 0 0), within narrower potential range. Similar well-defined increase in cathodic currents is also found for pure commercial RuO_2, as shown in Fig. 6b. Hence, these cathodic features could be an additional indication of higher RuO_2 content at the surface of RuO_2/TiO_2(8 0 0), which is assignable to proton injection into the hydrous structure of RuO_2 [39].

Although TGA measurements (Fig. 4) showed the negligible mass loss upon heating in air for RuO_2/TiO_2(8 0 0), the CV behavior changes considerably even with drying at 120 °C (Fig. 6b). The highest CV currents are registered for the USP as-prepared state, which decrease to almost one tenth upon annealing at 450 °C. The worsening of the capacitive performances upon heating could be associated to the changes of the state of oxides at the surface of spheres (Fig. 2b) and possibly to some aggregation of the RuO_2 at that surface. However, the worsening appears healed if the heating is applied to the coating on Ti (Fig. 6c), since the CV currents of both RuO_2/TiO_2(8 0 0)/Ti and RuO_2/TiO_2(2 0 0)/Ti are near twice of that of the corresponding annealed USP powders (Fig. 6a). Bearing in mind that there is the oxidation of Ti and consequently the generation of additional TiO_2 during the coating annealing, the healing/worsening appears strongly dependent on the TiO_2 stabilizing presence. It follows that TiO_2 migrates away from the aggregated RuO_2 sites toward the interior of the sphere when the powder is annealed. If USP powder at Ti substrate is heated, TiO_2 deficit at the sphere surface could be compensated from the Ti substrate oxidation. In order to check the mentioned influence of TiO_2, RuO_2/TiO_2(8 0 0) coating was prepared with the composition corrected to the EDX value for RuO_2/TiO_2(2 0 0) by the addition of $TiCl_3$ into RuO_2/TiO_2(8 0 0) powder suspension for coating preparation. The cyclic voltammogram of the RuO_2/TiO_2(8 0 0)/Ti coating with corrected composition (RuO_2/TiO_2(800 cc)/Ti) is shown in Fig. 6c. The currents are considerably increased upon correction and approaches the values registered for RuO_2/TiO_2(2 0 0) coating. This proves the considerations about healing influence of TiO_2 on the voltammetric properties of binary oxide.

Although the corrected composition was found to heal the CV response of RuO_2/TiO_2(8 0 0)/Ti toward CV-currents-promoting decrease of the USP temperature found for RuO_2/TiO_2(2 0 0)/Ti (Fig. 6a), there is a difference between CV currents between the two coatings in a wide potential range 0.0–0.9 V. Different morphology of the coatings, with much wider cracks of RuO_2/TiO_2(2 0 0)/Ti (Fig. 5), can influence considerably the capacitive response, causing different distribution of the capacitance through the coating. Different morphology can especially affect the coating anodic operation in brine electrolysis [7,24,38], when generated gaseous phase depletion dynamics takes place. This operation affects the stability and consequently service life of the anode.

To analyze stability of the prepared anode, the accelerated stability test was performed galvanostatically in diluted NaCl solution [38]. The relative change in cell voltage during the electrolysis is presented in Fig. 7.

RuO_2/TiO_2(2 0 0)/Ti is considerably more stable than the anodes prepared from USP powder synthesized at 800 °C. The loss of activity is indicated as gradual increase in cell voltage at the end of the anode service life. RuO_2/TiO_2(8 0 0)/Ti anodes are of rather poor stability, which is in accordance to previous report [20]. The correction of the coating composition in RuO_2/TiO_2(800 cc)/Ti improves the stability of the anode prepared from high-temperature USP powder only negligibly in comparison to RuO_2/TiO_2(2 0 0)/Ti of quite long service life. It appears that a weak healing of the stability is in the direction of improved CV currents (Fig. 6c) by correction of the coating composition, but not of considerable level.

The registered service life of RuO_2/TiO_2(2 0 0)/Ti is comparable to those of long-lasting anodes of similar coating (or particle in USP case) composition and amount [38,40]. These stability-related findings require additional analysis since the coating appearance is rather indented with respect to typical “cracked-mud” appearance [13,28,41], which should not be beneficial for the stability according to the

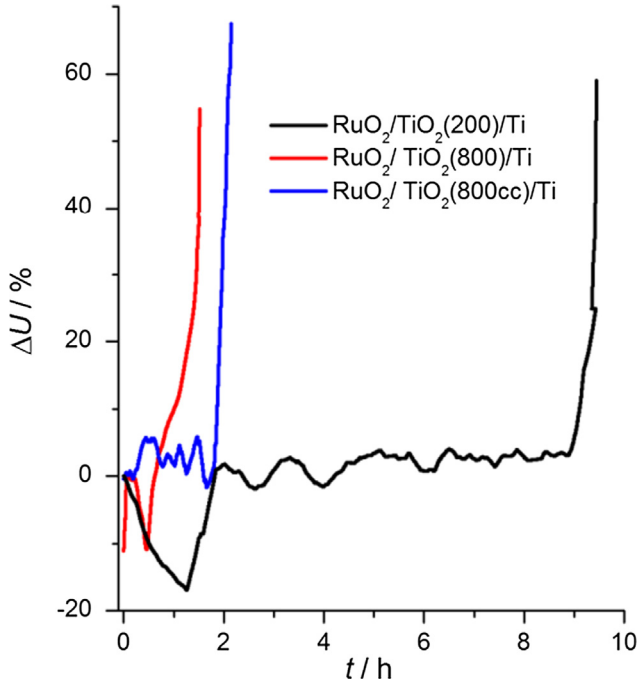

Fig. 7. The results of accelerated stability test of RuO_2/TiO_2(2 0 0)/Ti and RuO_2/TiO_2(8 0 0) in 0.5 M NaCl, pH 2, at 2 A/cm^2 and 18 °C. The end of service life is indicated by the relative increase in cell voltage, ΔU, by more than 50% with respect to initial value.

accepted mechanisms of the loss of ATA coating stability [7,24]. In addition, from the analyzed properties of RuO_2/TiO_2(2 0 0) and RuO_2/TiO_2(8 0 0) powders, related to their structure and composition, as well as from the structural and voltammetric similarities between the two coatings, considerable differences in stability of the anodes are hardly indicated. Most likely, the crucial key for the considerable improvement of the stability could be found in the analysis of structure-dependent distribution of the electrochemical properties throughout the coating layer. This analysis should be most conveniently performed by impedance measurements (EIS) [42,43], and subsequent EIS data analysis *via* transmission line equivalent electrical model [44].

EIS results, obtained at the open circuit potential, are shown in Fig. 8 as the capacitance complex plane plots (Fig. 8a) and corresponding distributions of the resistance and capacitance distribution down a transmission line equivalent circuit (TLEC, Fig. 8b).

Capacitance complex plane plots (CCPPs) shows the difference in capacitive features between the electrodes of the nominally the same composition (TiO_2-rich electrodes, RuO_2/TiO_2(2 0 0)/Ti and RuO_2/TiO_2(800 cc)/Ti) and that prepared from high-temperature USP powder rich in RuO_2 (RuO_2/TiO_2(8 0 0)/Ti). For RuO_2-rich electrodes, well-resolved capacitive semicircles in high frequency domain, down to *ca.* 1 Hz, is followed by the loops in low frequency domain. Only a loop is registered for RuO_2/TiO_2(8 0 0)/Ti electrode in whole frequency domain. The size of the loops (the values of the admittance imaginary component) indicate that RuO_2/TiO_2(8 0 0)/Ti should be of the lowest, whereas the sample prepared at low USP temperature is of highest capacitance. This finding agrees with the CV data given in Fig. 6, while the stability of the prepared anodes, Fig. 7, also follows the same order.

Different CCPP spectra from Fig. 8a obey the TLEC of a general form:

$$R_\Omega[R_L L](C_0(R_{p,1}(C_1(R_{p,2}(...(R_{p,n}C_n))))...)$$

where C_n relates to the capacitance available behind $\sum_{i=1}^{n} R_{p,i}$ resistance.

Ohmic resistance, R_Ω, and inductive elements, R_L and L in parallel, were required in series to a transmission line in order to quantify high

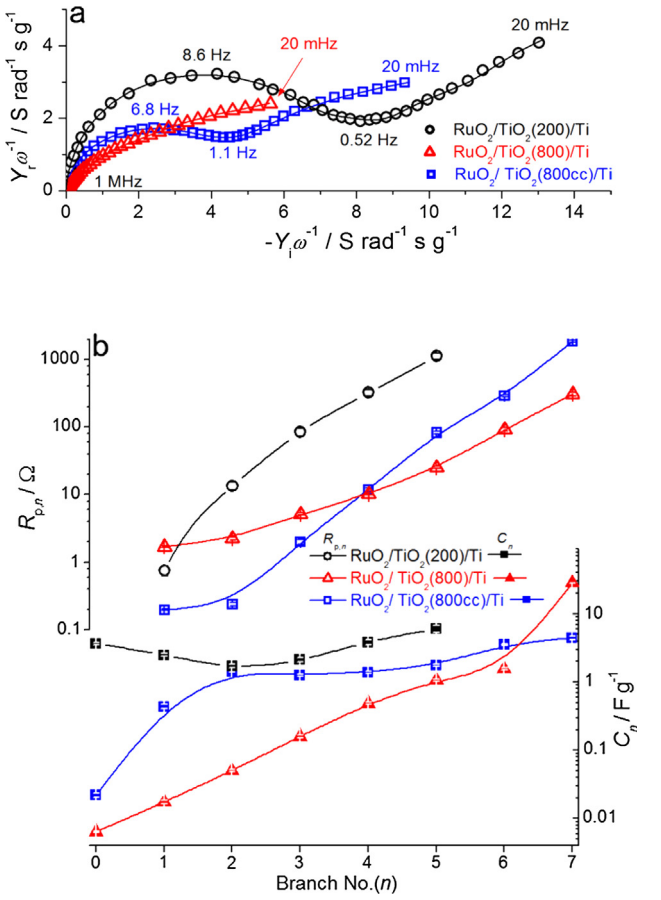

Fig. 8. (a) Capacitance complex plane plots (CCPPs) of the ATA coatings; 1 M H_2SO_4, open circuit potential; (b) resistance and capacitance distribution through the branches of transmission line equivalent circuits (TLEC) for investigated ATA coatings; impedance data of TLECs are presented as lines in CCPPs.

frequency EIS features. These parameters will not be analyzed further since they are intrinsic mostly to the measuring system. However, this extension of TLEC is required for the acquisition of the reliable values of other circuit parameters. As shown in Fig. 8b, 5 TLEC branches ($n = 5$) was enough for the fitting of EIS data of low-USP temperature sample, whereas the data of the samples prepared at high temperature required $n = 7$. This indicates that the structure, and consequently the distribution of electrical parameters, C_n and $R_{p,n}$, of (8 0 0)-samples is more complex. Required n values correlate to the appearances of the coatings, Fig. 5. Owing to much wider cracks of (2 0 0)-sample, more coating material is available for similar RC time domains (lower n) than in the case of (8 0 0)-samples with narrow cracks (higher n). Consequently, 3.6 F/g is readily available from RuO_2/TiO_2(2 0 0)/Ti as C_0, while RuO_2/TiO_2(8 0 0)/Ti delivers only 10 mF/g (Fig. 8b), despite higher amount of RuO_2 at the surface of the spheres (Table 1). The correction of the composition in RuO_2/TiO_2(800 cc)/Ti increases C_0 to 22 mF/g and considerably improves the capacitive response from 1st to 3rd branch, preceded by the decrease in $R_{p,1}$–$R_{p,3}$. The capacitance values from 2nd and 3rd branch almost reach the corresponding values for RuO_2/TiO_2(2 0 0)/Ti. However, it is to be noted that the correction of the coating composition affects neither capacitance nor the pore resistance for n above 4. It indicates that the elements for n 4–7 hence relate much to the interior of the spheres, where the composition of the mixed oxide is not affected by the addition of TiO_2. It follows that the highest registered capacitances (in CV, and high frequency domain as well) for RuO_2/TiO_2(2 0 0)/Ti is due to the response from up to $n = 2$ caused by intrinsic RuO_2/TiO_2 composition at the surface of the spheres from Fig. 5.

Bearing in mind the adopted causes for the loss of electrocatalytic activity [7,24] – namely, the structure-dependent competitive RuO_2 exhaustion from outer coating layers and TiO_2 interlayer generation by Ti support oxidation, the results from Figs. 7 and 8 can be correlated as follows. Owing to much higher amount of available sites for the reactions in stability test (seen as much higher capacitance values for $n = 2$, Fig. 8b), the real current density on RuO_2/TiO_2(2 0 0)/Ti is lower than on RuO_2/TiO_2(8 0 0)/Ti. This would cause the moderate RuO_2 exhaustion from the outer coating layers, and favored TiO_2 interlayer formation due to wider cracks during the electrolysis on RuO_2/TiO_2(2 0 0)/Ti. This involves the cell voltage as the main parameter which determines the anode service life, being in the field of cell geometry. Consequently, the increase in voltage, which follows the period of stable operation, is sudden for RuO_2/TiO_2(2 0 0)/Ti. On the other hand, the real current densities on the outer layers of 800 °C sample are considerably higher and causes fast and continuous exhaustion of RuO_2 from the coating surface. Owing to narrow cracks, the interlayer formation should be of lower importance for the stability than in the case of RuO_2/TiO_2(2 0 0)/Ti. Fast exhaustion rapidly generates TiO_2-rich surface layer of high resistance on the surface of RuO_2/TiO_2(8 0 0)/Ti, which is seen as rapid and continuous increase in cell voltage after short time of electrolysis (the period of stable operation is hardly found in Fig. 7). Although the operational features of the RuO_2/TiO_2(800 cc)/Ti in Fig. 7 is found more similar to the RuO_2/TiO_2(2 0 0)/Ti, the service life is healed only negligibly by the correction of the composition. This indicates that the mechanism of the stability loss for RuO_2/TiO_2(800 cc)/Ti could be mixed interlayer/outer-layer formation due to decreased pore resistance/increased active surface area ($n < 4$, Fig. 8b) with respect to RuO_2/TiO_2(8 0 0)/Ti.

Additional considerations related to conductivity and capacitance of the investigated coatings in their active and deactivated state are given as Supplementary material.

4. Conclusion

RuO_2/TiO_2 mixed oxide powders, consisted of spherically-shaped aggregates, were synthesized at two different temperatures (200 and 800 °C) by ultrasonic spray pyrolysis (USP). Low-crystalline powder was obtained at 200 °C, which is suitable for the preparation of highly stable coatings of activated titanium anodes (ATA). Synthesized USP powders consist much of separated anatase and rutile phases, with anatase structure preserved even at 800 °C in the core of spherical particles onto which crystalline RuO_2 preferentially grows. The USP temperature affects also the composition: high-temperature sample is of the sphere surface reach in RuO_2, as well as chloride–oxide conversion: both Ru species exist in low-temperature sample. The spherical structure is uniquely preserved in the ATA coatings prepared from USP powders, with that obtained from 200 °C sample expressing much wider coating cracks.

Despite incomplete oxide–chloride conversion, low crystallinity and lower surface RuO_2 content, low-temperature sample is of better electrochemical performances in comparison to 800 °C sample. Better performances are found also for ATA coating from 200 °C sample, and the key causes for this are related to Ti-rich mixed oxide composition and easier active surface area accessibility due to wider coating cracks. The highly pronounced differences in performances are found especially in ATA stability tests – the service life in electrolysis is considerably longer for the ATA from 200 °C sample. Detailed impedance measurements revealed that outer coating layers in case of 800 °C sample is of considerably smaller active surface area. Real current density at operational conditions of the stability test is hence considerably higher, *i.e.*, the rate of the RuO_2 exhaustion is faster in comparison to ATA from 200 °C sample. Consequently, ATA from 800 °C sample losses rapidly and continuously the activity in outer layers. ATA prepared from 200 °C sample ends service life suddenly once the defined coating/Ti substrate

TiO_2 interlayer is formed due to dominant penetration of the electrolyte through wide cracks towards the Ti substrate and its subsequent oxidation. It was found that the correction of the composition of the coating from 800 °C sample toward Ti-rich state of 200 °C sample increases the coating outer active surface area. Although the operational features of the composition-corrected ATA from 800 °C sample was found more similar to the ATA 200 °C sample, the service life is healed only negligibly by the correction of the composition.

Funding sources

Part of the research was supported by the funds of the bilateral research project, ID 451-03-01413/2016-09/7, supported by Deutsche Akademische Austausch Dienst (DAAD), Germany, and Ministry of Education, Science and Technological Development of the Republic of Serbia.

Acknowledgment

M.K., V.C., J.S. and V.P. acknowledge the financial support by the Ministry of Education, Science and Technological Development of the Republic of Serbia, Contract No. 172060.

Appendix A. Supplementary material

Supplementary data associated with this article can be found, in the online version, at https://doi.org/10.1016/j.apsusc.2018.09.066.

References

[1] S. Trasatti, Electrocatalysis: understanding the success of DSA, Electrochim. Acta 45 (2000) 2377–2385.
[2] X. Wang, R. Gordon, High-quality epitaxy of ruthenium dioxide, RuO_2, on rutile titanium dioxide, TiO_2, by pulsed chemical vapor deposition, Cryst. Growth Des. 13 (2013) 1316–1321.
[3] S. Ferro, M. Donatoni, A. De Battisti, V.N. Andreev, Adsorption of thallium cations on RuO_2–TiO_2 electrodes, J. Appl. Electrochem. 37 (2007) 1389–1394.
[4] V. Panić, A. Dekanski, S. Milonjić, V. Mišković-Stanković, B. Nikolić, Electrocatalytic activity of sol-gel-prepared RuO_2/Ti anode in chlorine and oxygen evolution reactions, Russ. J. Electrochem. 42 (2006) 1055–1060.
[5] C. Hu, H. Guo, K. Chang, C. Huang, Anodic composite deposition of $RuO_2{\cdot}xH_2O$–TiO_2 for electrochemical supercapacitors, Electrochem. Commun. 11 (2009) 1631–1634.
[6] V. Panić, A. Dekanski, R. Stevanović, Sol–gel processed thin-layer ruthenium oxide/carbon black supercapacitors: a revelation of the energy storage issues, J. Power Sources 195 (2010) 3969–3976.
[7] V. Panić, A. Dekanski, V. Mišković-Stanković, S. Milonjić, B. Nikolić, On the deactivation mechanism of RuO_2–TiO_2/Ti anodes prepared by the sol–gel procedure, J. Electroanal. Chem. 579 (2005) 67–76.
[8] Y. Wang, J. Guo, T. Wang, J. Shao, D. Wang, Y. Yang, Mesoporous transition metal oxides for supercapacitors, Nanomaterials 5 (2015) 1667–1689.
[9] P. Simon, Y. Gogotsi, Materials for electrochemical capacitors, Nat. Mater. 7 (2008) 845–854.
[10] H. Li, R. Wang, R. Cao, Physical and electrochemical characterization of hydrous ruthenium oxide/ordered mesoporous carbon composites as supercapacitor, Microporous Mesoporous Mater. 11 (2008) 32–38.
[11] Y. Xie, D. Fu, Supercapacitance of ruthenium oxide deposited on titania and titanium substrates, Mater. Chem. Phys. 122 (2010) 23–29.
[12] Y. Wang, Z. Wang, Y. Xia, An asymmetric supercapacitor using RuO_2/TiO_2 nanotube composite and activated carbon electrodes, Electrochim. Acta 50 (2005) 5641–5646.
[13] M. Aparicio, L. Klein, Thin and thick RuO_2-TiO_2 coatings on titanium substrates by the sol-gel process, J. Sol-Gel Sci. Technol. 29 (2004) 81–88.
[14] D. Suh, T. Park, W. Kim, I. Hong, Synthesis of high-surface-area ruthenium oxide aerogels by non-alkoxide sol–gel route, J. Power Sources 117 (2003) 1–6.
[15] B. Yao, L. Wang, C. Wang, Z. Wang, G. Yhao, Preparation and performances of RuO_2/TiO_2 films photocatalyst supported on float pearls, Chin. J. Chem. Phys. 20 (2007) 789–795.
[16] C.C. Hu, K.H. Chang, M.C. Lin, Y.T. Wu, Design and tailoring of the nanotubular arrayed architecture of hydrous RuO_2 for next generation supercapacitors, Nano Lett. 6 (2006) 2690–2700.
[17] S. Stopić, B. Friedrich, M. Schroeder, T. Weirich, Synthesis of TiO_2 core/RuO_2 shell particles using multi step ultrasonic spray pyrolysis, Mater. Res. Bull. 48 (2013) 3633–3635.
[18] Y.-G. Wang, X.-G. Zhang, Preparation and electrochemical capacitance of RuO_2/TiO_2 nanotubes composites, Electrochim. Acta 49 (2004) 1957–1962.
[19] Y. Xie, L. Zhou, C. Huang, Y. Liu, J. Lu, Preparation and electrochemical capacitance of ruthenium oxide-titania nanotube composite, Mater. Sci. Forum 614 (2009) 235–241.
[20] M. Košević, S. Stopic, A. Bulan, J. Kintrup, R. Weber, J. Stevanović, V. Panić, B. Friedrich, A continuous process for the ultrasonic spray pyrolysis synthesis of RuO_2/TiO_2 particles and their application as a coating of activated titanium anode, Adv. Powder Technol. 28 (2017) 43–49.
[21] S. Stopic, Synthesis of Nanosized Particles by Ultrasonic Spray Pyrolysis, Shaker Verlag GmbH, Germany, 2015.
[22] J.C. Forti, P. Olivi, A. De Andrade, Characterisation of DSA®-type coatings with nominal composition $Ti/Ru_{0.3}Ti_{(0.7-x)}Sn_xO_2$ prepared via a polymeric precursor, Electrochim. Acta 47 (2001) 913–920.
[23] Z. Yi, C. Kangning, W. Wei, J. Wang, S. Lee, Effect of IrO_2 loading on RuO_2–IrO_2–TiO_2 anodes: a study of microstructure and working life for the chlorine evolution reaction, Ceram. Int. 33 (2007) 1087–1091.
[24] V.M. Jovanovic, A.B. Dekanski, P. Despotov, B.Z. Nikolic, R.T. Atanasoski, The roles of the ruthenium concentration profile, the stabilizing component and the substrate on the stability of oxide coatings, J. Electroanal. Chem. 339 (1992) 147–165.
[25] M.L. Foo, Q. Huang, J.W. Lynn, W.-L. Lee, T. Klimczuk, I.S. Hagemann, N.P. Ong, R.J. Cava, Synthesis, structure and physical properties of Ru ferrites: $BaMRu_5O_{11}$ (M = Li and Cu) and $BaM'_2Ru_4O_{11}$ (M' = Mn, Fe and Co), J. Solid State Chem. 179 (2006) 563–572.
[26] D.A.H. Hanaor, I. Chironi, I. Karatchevtseva, G. Triani, C.C. Sorrell, Single and mixed phase TiO_2 powders prepared by excess hydrolysis of titanium alkoxide, Adv. Appl. Ceram. 111 (2012) 149–158.
[27] K. Kameyama, S. Shohji, S. Onoue, K. Nishimura, K. Yahikozawa, Y. Takasu, Preparation of ultrafine RuO_2 - TiO_2 binary oxide particles by a sol-gel process, J. Electrochem. Soc. 140 (1993) 1034–1037.
[28] S. Trasatti, W.E. O' Grady, Properties and applications of ruo_2-based electrodes, in: H. Gerisher, C.W. Tobias (Eds.), Advances in Electrochemistry and Electrochemical Engineering, Wiley & Sons Inc., New York, 1981, p. 177.
[29] A.A. Davydov, Molecular Spectroscopy of Oxide Catalyst Surfaces, Wiley, England, 2003.
[30] P.R. Deshmukh, R.N. Bulakhe, S.N. Pusawale, S.D. Sartale, C.D. Lokhande, Polyaniline–RuO_2 composite for high performance supercapacitors: chemical synthesis and properties, RSC Adv. 5 (2015) 28687–28695.
[31] A.A. Ismail, L. Robben, D.W. Bahnemann, Study of the efficiency of UV and visible-light photocatalytic oxidation of methanol on mesoporous RuO_2-TiO_2 nanocomposites, ChemPhysChem 12 (2011) 982–991.
[32] Y.J. He, J.F. Peng, W. Chu, Y.Z. Li, D.G. Tong, Black mesoporous anatase TiO_2 nanoleaves: a high capacity and high rate anode for aqueous Al-ion batteries, Mater. Chem. A. 2 (2014) 1721–1731.
[33] J.M.H. Enríquez, L.A.C. Lajas, R.G. Alamilla, E.Á. San Martín, P.G. Alamilla, E.B. Handy, G.C. Galindo, L.A.G. Serrano, Synthesis of solid acid catalysts based on TiO_2-SO_4^{2-} and Pt/ TiO_2-SO_4^{2-} applied in n-Hexane Isomerization, Open J. Metal 3 (2013) 34–44.
[34] S. Mali, C. Betty, P. Bhosale, P. Patila, Synthesis, characterization of hydrothermally grown MWCNT–TiO_2 photoelectrodes and their visible light absorption properties, ECS J. Solid State Sci. Technol. 1 (2012) M15–M23.
[35] C. Zhang, H. Zhou, X. Yu, D. Shan, T. Ye, Z. Huang, Y. Kuang, Synthesis of RuO_2 decorated quasi graphene nanosheets and their application in supercapacitors, RSC Adv. 4 (2014) 11197–11205.
[36] A. Cornell, B. Håkansson, G. Lindbergh, Ruthenium based DSA® in chlorate electrolysis—critical anode potential and reaction kinetics, Electrochim. Acta 48 (2003) 473–481.
[37] J. Pietron, M. Pomfret, C.N. Chervin, J.W. Long, D.R. Rolison, Direct methanol oxidation at low overpotentials using Pt nanoparticles electrodeposited at ultrathin conductive RuO_2 nanoskins, J. Mater. Chem. 22 (2012) 5197–5204.
[38] V. Panić, A. Dekanski, S. Milonjić, R. Atanasoski, B. Nikolić, Influence of the aging time of RuO_2 and TiO_2 sols on the electrochemical properties and behavior for the chlorine evolution reaction of activated titanium anodes obtained by the sol-gel procedure, Electrochim. Acta 46 (2000) 415–421.
[39] S. Ardizzone, S. Trasatti, Interfacial properties of oxides with technological impact in electrochemistry, Adv. Colloid Interf. Sci. 64 (1996) 173–251.
[40] F. Moradi, C. Dehghanian, Addition of IrO_2 to RuO_2+TiO_2 coated anodes and its effect on electrochemical performance of anodes in acid media, Prog. Nat. Sci.-Mater. 24 (2014) 134–141.
[41] A.R. Zeradjanin, F. La Mantia, J. Masa, W. Schuhmann, Utilization of the catalyst layer of dimensionally stable anodes—interplay of morphology and active surface area, Electrochim. Acta 82 (2012) 408–414.
[42] V.V. Panić, T.R. Vidaković, A.B. Dekanski, V.B. Mišković-Stanković, B.Ž. Nikolić, Capacitive properties of RuO_2-coated titanium electrodes prepared by the alkoxide ink procedure, J. Electroanal. Chem. 609 (2007) 120–128.
[43] G. Šekularac, M. Košević, A. Dekanski, V. Djokić, M. Panjan, V. Panić, High energy/power supercapacitor performances of intrinsically ordered ruthenium oxide prepared through fast hydrothermal synthesis, ChemElectroChem 4 (2017) 2535–2541.
[44] G. Paasch, The transmission line equivalent circuit model in solid-state electrochemistry, Electrochem. Commun. 2 (2000) 371–375.